Lakangaon: a unique and anomalous, non-cumulate eucrite?

H. Thakur[1], D. Ray[2*], R. Chakrabarti[1], and S. Ghosh[3]

[1]Centre for Earth Sciences, Indian Institute of Science, Bangalore, 560012, India

[2]Physical Research Laboratory, Ahmedabad, 380009, India

[3]54/3 Mahendra Banerjee Road, Kolkata, 700 060, India

(For correspondence: dwijesh@prl.res.in/dwijeshray@gmail.com)

Abstract

The Fe-rich Lakangaon eucrite is a highly recrystallized, monomict fragmental breccias with some noticeable anomalous petrochemical characteristics. The texture of the Lakangaon breccia reflects a polyphase, post-igneous history of thermal and impact metamorphism corresponding to a coarse-grained lithic and mineral clast of variable size embedded in a finer recrystallized clastic matrix. The majority of lithic clasts are coarse-grained, gabbroid textured with some granulitic hornfels mosaic look, heavily fractured with subsequent healing recoveries. The signatures of brittle rupturing and displacements and prominent kink bands due to flexure slip deformation in the exsolution lamellae of pyroxenes are also common. The absence of impact melt and the lack of Ni-free iron beads or Ni-bearing metal grains, along with a low abundance of siderophile elements in Lakangaon, probably rule out the possibility of any chondritic contamination. Lakangaon shows two types of post-accretionary modifications: mechanical mixing during impact and thermal alterations before, during and after the impact. Evidences of at least two phases of impact history are recorded: (a) the first impact-induced heat causes recrystallization and equilibration of pyroxenes with structural inversions from pigeonite to orthopyroxene. Further, subsolidus cooling resulted in pigeonite with exsolved augite lamellae and ductile to brittle fracturing in the pyroxenes and plagioclase clasts, (b) the second impact phase during the post-crystallization period resulted in the occurrence of fractured clasts along with vaporization of troilites. The post-impact thermal annealing induced further coarsening of recrystallized clasts, formation of granulitic hornfels textures in the clasts, healing of earlier cracks and fractures within the clasts and finally, formation of clouding textures. The sulphur vapour played a significant role as a transport medium for the extensive development of clouding texture at a late stage.

Keywords: Lakangaon, non-cumulate eucrite, fragmental breccia, HED meteorites, impacts

Introduction

Howardite-Eucrite-Diogenite (HED) meteorites are the largest achondrite groups and have been thought to originate from parent body 4 Vesta (Mittlefehldt, 2015). The HEDs are the only meteorite group where the linkage between the meteoroids and their parent body has been established (McSween et al., 2013). The crust of Vesta, in the form of eucrites, provides the opportunity to study the earliest basaltic volcanism, the origin of the primordial crust in the early solar system, and also offers to examine the magmatic process involving small, differentiated asteroid bodies (Barrat et al., 2007). The non-cumulate and cumulate eucrites are generally considered to be the crust of the differentiated body Vesta, while Howardites are complex impact breccia containing predominantly Eucrite and Diogenite clasts. The diverse clast suites within the two ends clans-monomict/polymict eucrite, and monomict/ polymict diogenite build up a continuous sequence of polymict breccias, variously termed as eucrite-enriched howardite, normal howardite and diogenite-enriched howardites. The petrogenesis of Vestan igneous rocks is intriguing and not well-constrained yet. New major, trace, and REE data of the least studied HED meteorite fall samples will always be an important contribution to infer the magmatic process and the textural intricacy of the Vestan magma.

In meteoritics, the term ‘anomalous’ means unusual and thus represents a category for mismatch samples concerning the traditional well-established pigeon-hole classifications. Unusual mineralogy, unusual textures, unusual bulk composition and mismatch among any of these parameters could be the possible causes of anomaly. To mention a few, Ibitara is a basaltic eucrite with very high-Ti bearing chromite (TiO_2: 15 to 24 wt%). Pasamonte is a basaltic eucrite with unusually Al_2O_3 - rich chromite (Al_2O_3: ~17.7 wt%). Millibillie is a basaltic eucrite with unusually low TiO_2 bearing chromite (TiO_2 ~ 2 wt%). Pomozdino, unusually rich in magnesium, is a ‘partial cumulate eucrite’ with ~20 to 40 wt% cumulus minerals in a substantial amount of solidified melt. The Lakangaon eucrite has not drawn much attention as

compared to other known Indian eucrites for its limited main mass and heterogeneous nature. Lakangaon is classified as monomict eucrite breccias in the Meteoritic Bulletin (2006, v.7.1), one of 274 approved meteorites as of date. In this study, our detailed petrochemical studies suggested Lakangaon as an 'anomalous' type for its cumulate-like texture and mineralogy, which is mismatched with its basaltic eucrite bulk chemical composition.

Coulson (1940), in his memoir, described the eye-witness account of the Lakangaon meteorite fall (21º52´N; 76º02´E) on November 24, 1910 around 18:00 hrs in Nimar region of British India, presently in Khandwa district, Madhya Pradesh, India. As per the Geological Survey of India (GSI) report, there were only two small fragments of 125.06 gm and 87.5 gm, respectively with a total weight of 212.6 gm registered. Duke and Silver (1967) classified Lakangaon as a monomict cumulate eucrite based on its pyroxene mineralogy, whereas it is classified as an extremely iron-rich, non-cumulate eucrite following Nuevo Laredo trend in bulk chemical composition (McCarthy et al., 1974; Warren et al., 1985; Barrat et al., 2000). Lakangaon, being a lesser-known Fe-rich eucrite, we undertook a holistic approach to identify the igneous processes based on a new set of data on the mineralogy and textural features in addition to whole-rock chemistry, both of which are always considered the keys to understanding magmatic crystallization event of the parent body. Our new findings on Lakangaon eucrite may help to constrain the thermal and chemical evolution of 4 Vesta.

Macroscopic description of samples

Before petrological studies, a hand specimen study of the two small fragments of Lakangaon in the repository of GSI was felt relevant by one of us (SG) for its flight markings and other surface textures developed in the atmosphere along the lines of Krinov (1960). The overall shape of Lakangaon's main mass (5.1 cm × 5.0 cm × 3.2 cm) is a part of a trigonal pyramid with one highly glossy, pitch-black, closely netted face and one dull brown, oxidized

face. Fusion crust (0.2-0.4 mm thick) shows faint flowage and peeling off in some patches. (Fig. 1). The specimen is fresh in terms of the degree of weathering (A) and shows negligible fracturing (A) according to the criteria after Gooding (1986), except for some shrinkage cracks in the crust. It is marked with a prominent, nearly circular (~1 cm diameter), shallow regmaglypt, and one prominent groove due to the removal of clast at the point of intersecting fractures. The interior of the specimen appears brecciated with a few isolated clasts amidst a fine-grained greyish matrix. One of the flat fractured surfaces is limonitic brown for sulphide alterations. It is interpreted from the flowage texture and maximum oxidation in fusion crust that dull face formed at the front/lateral side during its last stage of atmospheric flight.

Analytical Techniques

All petrographic characterization, textural observation, and back-scattered electron (BSE) image analysis of all the polished thick and thin sections were conducted using a Field Emission Electron Probe Microanalyser (FE-EPMA; JEOL 8530F Plus, Japan) with Energy Dispersive X-ray Spectrometer (EDS) and five Wavelength Dispersion Spectrometer (WDS) at Physical Research Laboratory (PRL), Ahmedabad, India. The operating condition employed was a typical accelerating voltage of 15 keV and 15 nA sample current and beam size of 1 micron. Natural and synthetic mineral standards are used for calibration and include Si (Diopside), Mg (Olivine), Ti (Rutile), Al (Kyanite), Fe (Magnetite), Cr (Cr_2O_3), Mn (Rhodonite), Na (Albite), K (Orthoclase), P (Apatite), S (Pyrite), Ni (Ni metal), Co (Co metal). Before the microprobe analysis, all section mounts were gold-coated and imaged at a range of magnification. The BSE images were pieced together to make a complete mosaic map of each section mount.

The sample was powdered using agate mortar and pestle for the bulk major and trace element composition. Approximately 10 mg of sample powder was dissolved in a 15 ml screw-cap Teflon vial from Savillex using a mixture of 1 ml concentrated HNO_3 and 1 ml concentrated

HF acids. After 48 hours, the acid mixture was evaporated, and a mixture of 1 ml concentrated HNO_3, and 1 ml concentrated HCl was added to the sample. After another 48 hours of reaction at 100 degrees Celsius, the Teflon vials were opened for evaporation, and the residues were dissolved in 2 ml of HNO_3. Two separate 125 ml pre-cleaned HDPE bottles (from Tarsons) were used for each sample for making trace elements aliquots with a dilution factor of $\sim$4,000 and a major elements aliquot with a dilution factor of $\sim$10,000. The dilution was carried out using 18.2 MΩ water. Sample preparation was executed in class 10k clean lab at the Centre for Earth Sciences (CEaS), Indian Institute of Science (IISc), Bangalore. Elemental concentrations were measured using a quadrupole Inductively Coupled Plasma Mass Spectrometer (ICP-MS, Thermo Scientific X-Series II) at CEaS, IISc, equipped with skimmer cones. A CETAC ASX-520 auto-sampler was used. The uptake time for samples and standards was 50 seconds, while the rinse time was 90 seconds (in 2% HNO_3). The CeO^+/Ce^+ ratio was kept below 0.5% to minimize oxide-related interferences to eradicate the possibility of oxide-related interferences, which affect the measurements of some of the middle to heavy-REEs. All raw counts were corrected for the contribution from acid blanks. USGS rock standards BHVO-2 (Hawaiian basalt), AGV-2 (Guano Valley Andesite), and BCR-2 (Columbia River basalt). The accuracy of the data was tested by analyzing USGS rock standard BIR-1 (Icelandic basalt) run as an unknown. The reproducibility for trace and major element concentration data is better than 5% for most elements.

Results

Petrography

A mosaic of back-scattered images (BSE) of the polished mount (4.2 mm X 3 mm) confirms its overall texture of a typical monomict breccias comprising loosely welded subangular to subrounded lithic clasts of variable size (largest one measures max 1.5 mm X 0.55 mm)

embedded in a finely crushed, comminuted and pulverized, partly to completely recrystallized silicate matrix (Fig. 2). A detailed petrography of the clast components and the matrix components are individually dealt in the subsequent paragraphs to decipher the mineralogy and textures of Lakangaon eucrite and their subsequent alterations.

Clast component

Six larger clasts (Clast A to Clast F) were examined in detail for the mineralogy and texture. The overall nature of all the clasts suggests a similar mineralogy and texture comparable with that of clinopyroxene-enriched gabbroic basalt or a cumulate eucrite (Fig. 2). All the clasts are also thermally metamorphosed showing evidence of no chemical zoning, equant grains with triple point interfaces, hornfels texture and subsolidus exsolution lamellae in pyroxene grains. Further, the deformed texture of the exsolved pyroxenes, in addition to kink bands at multiple points, is a common feature (Fig. 3a). Considerable attrition, even after brecciation caused by impact, is evident from variable size and subangular to subrounded shapes of the clasts amidst cataclastic texture of the matrix (Figs.2, 3b). In general, it is essentially a coarsely recrystallized cumulate aggregate of clinopyroxene (~ 40-60 vol%), plagioclase (~10-40 vol%), free silica (~5-20 vol%) along with minor accessories of ilmenite, chromite and troilite (~1.5-4 vol%). The presence of silica (5-20 vol %), and the availability of limited zircon grains as primary constituents within the gabbroic cumulate clasts are noteworthy.

In Lakangaon, both pyroxene and plagioclase grains of the cumulate are overprinted with a variety of large and tiny inclusions of ilmenite, chromite, silica and occasionally troilite, besides individual occurrences of all the minor accessories. In pyroxenes, the clouding-causing minerals are thin and rod-shaped and are mostly aligned in one direction. The inclusions range from 0.2 × 0.05 µm to 1.8 × 0.5 µm (Fig. 4a). In contrast, the clouding pattern in plagioclase

shows inclusions of various sizes (average ~ 1.1 X 1.3 µm), from almost circular to triangular and even rectangular (Fig. 4b-d).

In order to ascertain the cloud-causing mineral phases occurring as tiny inclusions in both pyroxenes and plagioclase, we employed BSE image segmentation using a K-means clustering algorithm for each image to demonstrate different phases with unique labels (colors). To provide the best possible distinction between phases, the labels of the phases were not selected in ascending order (default), but rather the colour for each phase was carefully chosen for easy distinction of phases. The colour scheme is as follows: for cracks and crevices: 1 (navy blue), silica: 3 (sapphire blue), plagioclase: 4 (light blue), augite: 6 (light green), pigeonite: 7 (yellow), chromite: 8 (orange), ilmenite: 9 (red), and troilite: 10 (brown). In some cases, the peaks of different phases overlap with each other, especially with augite and pigeonite; otherwise, the peaks of metallic phases, plagioclase, and silica are clear and do not overlap with each other. It implies that even after manual tweaking of the parameters, the demarcation between augite and pigeonite remains unresolved, especially near the edges of the grains, where the pixel values gradually change.

By analyzing multiple images through this algorithm, it is understood that there is a difference between clouding in pyroxene and plagioclase. The plagioclase in Lakangaon is clouded primarily with pyroxenes (both augite and pigeonite) and secondarily with silica; a few clusters of chromite and troilite inclusions are present, especially near a big chromite inclusion and towards the edges of the grain, respectively. The silica inclusions are localized and do not show much scatter. Instead, they mostly occur as thin, small blebs, in straight or curvy lines within the plagioclase. Ilmenite inclusions are mostly anhedral but in some places, with perfect square/rectangular shapes. A thin, straight line/streak can also be observed, which is entirely made up of these clouding-causing minerals and looks like a dashed line (Figs. 5a, b). Troilite occurs as very fine (< 0.5 μm), mostly rod and bleb-shaped inclusions in exsolved pyroxenes

and causes clouding though troilite and ilmenite grains of size >10 μm are present as relatively large inclusions in pyroxenes as well (Fig. 5 c).

Pyroxenes of Lakangaon, unlike all other eucrites, are all exsolved type and Fe-enriched with lamellae width of augite ranging between < 0.1 µm to 4 µm irrespective of its occurrence in large clasts or the finer matrix. It is essentially homogenous Fe-pigeonite that has undergone both exsolution and inversion. In pyroxene quadrilateral diagram, compositional plots of Lakangaon pyroxenes define a distinct linear trend at uniformly constant En_{30} mol% and Wo-content inversely decreases with Fs- content giving rise to a pyroxene composition variation in two distinct clusters: host pyroxene around Fe-pigeonite + inverted Fe-orthopyroxene and the other as the cluster of exsolved lamellae around Ca-rich Fe-augite. On closer inspection, we find two types of exsolved pyroxenes: (1) Relatively thick lamellae of ferroaugite in the Fe-pigeonite host and (2) relatively fine lamellae of ferroaugite in the host of pigeonite inverted Fe-orthopyroxene (Table 1). Following the classification of eucritic pyroxenes proposed by Miyamoto et al. (1978), Lakangaon pyroxenes belong to the Moore County type, implying a slower cooling rate, generally expected in gabbroic clasts of cumulate eucrites. In contrast, the linear compositional trend of Lakangaon pyroxenes closely matches with the trend of Nuevo Laredo basaltic eucrites in the 'Pyroxene Ternary diagram' (Fig. 6). Lakangaon pyroxenes closely match with Type 6 eucrite of Takeda and Graham (1991) where type 1 is pristine basalt with original igneous zoning preserved and type 6 is reheated and extensively metamorphosed eucrites showing clouding of inclusions, both inverted and exsolved pigeonites with few µm thick augite lamellae.

Plagioclase feldspar occurs within the clasts as well as in the matrix (Fig. 7). Plagioclase content beyond ~40 vol% is an index to cumulate eucrite. Lakangaon eucrite, which is pyroxene dominated with plagioclase content between 10 vol% and 40 vol%, clearly suggests its basaltic affinity. Texturally, separate aggregates of plagioclase in subrounded to irregular

clasts resemble brecciated, gabbroic texture, though plagioclase also occurs as laths in pyroxenes. In general, it is ternary calcic plagioclase of bytownite-anorthitic composition ($An_{82.19-89.99}$) with a subtle compositional gap in the 'Feldspar Ternary diagram' between the clast and the matrix (Table 2, Fig. 7).

Free silica grains, unusually abundant up to ~20 vol%, are present as either inclusions or intergrowth with pyroxene and plagioclase. It is compositionally ~ 99% pure.

Chromite occurs in Lakangaon as inclusions in pyroxenes, plagioclase, and also in silica. It is relatively smaller in size as compared to ilmenite, mostly anhedral, and most grains are of the size between 2 μm and 10 μm, with some grains up to 75 μm in association with ilmenite (Fig. 8a). All these chromites are extremely Fe-rich chromite with <10 % Al, ~50% Fe^{3+} and ~50% Cr (Table 3). These are classified as chromian pleonaste when classified in the Fe/ (Fe + Mg) vs Cr / (Cr + Al) diagram.

Ilmenite, exclusively present in the clasts, are relatively large inclusions in pyroxenes as well as in plagioclase, sometimes also in association with silica, in various shapes and sizes (up to 150 μm x 100 μm), from subhedral to euhedral to wide elongated (bottle-like) shape. Ilmenite also occurs as individual grains, and composite grains with chromite (Fig. 8a). Ilmenites are compositionally uniform with ~ 53% TiO_2 and ~ 45% FeO and minor Si, Ca, Mg, and Cr (Table 3).

Troilite occurs as very fine inclusions in pyroxenes and causes clouding. The composition of troilite is pure FeS with Co, Cr, and Ni below detection limits (Table 3). It is mostly rod and bleb-shaped when occurring in clouding (< 0.5μm), and it is mostly anhedral with a size of < 10 μm when it exists as a discrete grain.

In Lakangaon, zircon grains occur as accessory phases and appear euhedral, nearly euhedral, and subhedral in shape and size, ranging between 8 μm and 12 μm in size. Often, zircon is

found to be associated with either ilmenite or as isolated grains near ilmenites (Fig. 8b). It is interesting to note that all the zircons are nearly uniform in Zr content (65- 67 wt% ZrO_2) whereas zircons associated with ilmenites are rich in both FeO (1.49 - 1.67 wt%) and TiO_2 (0.30- 0.39 wt%) compared to those of isolated grains.

Nature of the Matrix component

Matrix component, widely distributed around the clast peripheries as well as in between the clasts (Fig. 3b), is a cataclastic aggregate of clast components with similar exsolved pyroxenes and bytownite plagioclase (Fig. 7). Pyroxene is more abundant than plagioclase and pyroxenes are compositionally Fe pigeonite with variable FeO (19.8- 37.9wt %), TiO_2 (0.09- 0.29 wt%) and CaO (2.3- 20.0) wt%. Ophitic to subophitic intergrowth textures between plagioclase laths and pigeonites are rare. Additionally, several prominent pulverized zones showing loss of birefringence, anomalous interference colors, and kink bands in pyroxene in the vicinity of thick (0.01 to 0.06 mm) fractures in thin section microscopy are also noted as the products of the attritional process. The anomalous nature of textures between the clast and the matrix components of Lakangaon monomict breccia is comparable with that of the "Eucrite-type" achondrites from Mittlefehldt et al. (2022).

Whole-rock geochemistry

Eucrites are divided into cumulates and non-cumulates based on the chemical makeup of the whole meteorite. These two groups separate themselves in the TiO_2 vs FeO*/MgO diagram (Fig. 9). The plot further segregates the basaltic eucrites into two distinct trends, the Main-Group Nuevo Laredo (MGNL) trend and the Stannern trend (Barrat et al., 2003, Barrat et al., 2007). Lakangaon falls under the MGNL trend of basaltic eucrite. Lakangaon, known for its highest bulk Fe content, shows greater FeO*/MgO and TiO_2 content values.

The chondrite normalized REE data (normalized data from McDonough and Sun, 1995) shows an almost flat pattern (La/Yb_n = 0.94) (Fig 10, Table 4). The total REE content (52.49 ppm) also ranges intermediate between cumulate and non-cumulate eucrite. However, the LREE shows a slightly increasing trend from La to Sm (La/Sm_n = 0.98), a significant negative Eu anomaly (Eu/Eu* = 0.78), and then again, a relatively flat pattern from Gd to Yb (GD/Yb_n = 0.84). The pattern matches the Lakangaon data measured by Barrat et al., 2000.

Discussion

Generally, all monomict eucrite breccias contain only one type of pyroxene, that is, pigeonite in almost all the clasts, and such a sample represents a small vertical depth within the parent body. Genomict breccias in eucrites are very rare, and their clasts contain two or more types of pyroxenes, implying sampling up to a few km of depth in the parent body. The Lakangaon falls well into the category of 'monomict breccia'.

Eucrites are texturally classified into cumulate and non-cumulate types. Cumulate eucrites are generally unbrecciated, medium to coarse-grained, equigranular aggregate of pyroxene and plagioclase where plagioclase may be dominant or nearly in subequal amount with pyroxenes. The primary texture is gabbroic, and it may show the preferred orientation of crystals for gravity settling under slow cooling. These eucrites are generally undersaturated magma with normative olivine, a variable amount of normative plagioclase and free SiO_2 in the form of quartz or tridymite and characterized by wide variation in FeO*/(FeO + MgO) in bulk chemistry. Plagioclases are more calcic, and pyroxenes are less ferrous. The main pyroxene is inverted pigeonite with very common microscopic to submicroscopic exsolution textures that exhibit Ca-rich augite pyroxenes in a Ca-poor pigeonite host. In a rapidly cooled mafic magma, monoclinic pigeonites are common, whereas in slowly cooled mafic magma like gabbro, structural inversion of monoclinic pigeonite to orthorhombic pyroxene takes place through a 'massive transformation' mechanism. In such inversion, Fe-pigeonites will be inverted to Fe-

rich orthopyroxene, and excess Ca will be present as augite blebs or exsolved phases in association with orthopyroxene. The extent of these two processes, exsolution and inversion depends upon the cooling rate. About the general characterization of cumulate eucrites, we note our Lakangaon as pyroxene-dominated gabbro representing slowly cooled mafic magma. Moreover, the Lakangaon pyroxenes are equilibrated with similar compositions both in the clast and in the matrix, whereas its plagioclase compositions are not so well equilibrated for the subtle difference between the clast and the matrix.

Non-cumulate eucrites, also called Main Group (MG) eucrites or Nuevo Laredo (NL) eucrites, are commonly monomict breccias. If unbrecciated or least metamorphosed, primary igneous melt textures like Flow texture, vesicular structure, fine-grained basaltic ophitic and subophitic textures, chemical zoning in pyroxenes could be available in relict forms within the ferrous pyroxene-dominated basaltic clasts where less calcic plagioclase content varies between 12 vol% and 40 vol%. Pyroxenes show a restricted composition nearly $En_{25\text{-}30}$ mol%. The Wo- content inversely decreases with Fs- content, and yields a pyroxene composition variation from pigeonite to subcalcic augite and ferroaugite. In this context, the typical fine-grained basaltic texture is missing in Lakangaon, although it lacks no other primary texture, structure, or zoning. Chemically, the non-cumulate eucrite magmas are silica saturated, consistently quartz normative with the presence of excess SiO_2 in the form of tridymite and uniform normative plagioclase, Ab ~10±5 mole%. It is characterized by limited variation in bulk composition marked by a cluster of FeO*/(FeO + MgO) mol% at ~60 ± 3. Lakangaon resembles the non-cumulate eucrites with some deviations, especially in REEs (Fig. 10).

The ‘Clouding texture’ is developed due to the presence of very finely disseminated inclusions in both pyroxenes and plagioclase grains and is generally common in many of the eucrites. Duke and Silver (1967), Dymek et al (1976), and Stolper (1977) explained this clouding process as a result of inclusions during crystallization and subsequent thermal metamorphism,

but Harlow and Klimentidis (1980) noted that the 'Clouding texture' in basaltic eucrites is abundant in healed microfractures, twin boundaries, and exsolution lamellae interfaces in pyroxenes as blebs, rods, lenses of mostly ilmenite and chromite and rarely of plagioclase, silica phase, Ni- free Fe metal and troilite. The Plagioclase grains are clouded with rods and blebs of mostly high Ca pyroxene and a variable amount of Ni-free Fe metal, silica phase, chromite, and ilmenite. They interpreted 'clouding' to be the result of the exsolution of minor components that became incompatible and crystallized on microfractures and other nucleation sites during post-brecciation metamorphism (subsolidus reheating event). Two prerequisites for the origin of clouding include (a) reduction of silicate FeO to metallic Fe in both pyroxene and plagioclase and possible redox of Cr^{2+} to Cr^{3+} in pyroxenes. Clouding is considered a useful indicator of post-crystallization events subjected to water-free reducing metamorphism.

The clouding is extremely intensive in Lakangaon, and almost every pyroxene grain is clouded to a lesser or greater extent (Fig. 4). This might be related to the fact that Lakangaon is among the most Fe-rich eucrite as more Fe content in pyroxene might involve more leaching of troilite. Another noticeable feature in the clouded pyroxenes from Lakangaon is that the exsolved lamellae of augite are not continuous from one end to another and look shifted and deformed multiple times in between, which might be an act of some microfractures that later got healed. In most pyroxene grains, apart from one or two big cracks that go almost through the grain, a few mini-fractures can also be seen. It is plausible that those micro-fractures were where the inclusions had formed, and the micro-fractures eventually healed, designated as "healed cracks" (Metzler et al. 1995). The clouding-causing troilite inclusions in the pyroxenes of Lakangaon are all rod and bleb-shaped.

The presence of silica (5 to 21 vol %) in the gabbroic clasts as one of the primary constituents is noteworthy; it could be due to either the crystallization of quartz normative basaltic magma or the assimilation of silicic components.

Zircon grains of Lakangaon are largely noted in large gabbroic clasts and some of these are closely associated with ilmenite accessories. All these zircons are small (8 to 12 μm), nearly euhedral to euhedral with hexagonal outline and with no signature of metamorphism (Fig. 8). Zircons interfaced with ilmenite grains compositionally reflect higher TiO_2 content compared to those of individual grains. According to Haba et al. (2014), zircons from basaltic eucrites must have originated in melts that were saturated in Zr and Si. These melts can occur as a result of the crystallization of constituent minerals like clinopyroxene and plagioclase; moreover, smaller grain size (< 20 μm) of zircons generally suggest that these are unrelated to any thermal event caused by metamorphism.

McCarthy et al. (1974) first published the bulk major element composition of Lakangaon eucrite from a 0.5 mg powdered sample by XRF analytical technique. It was similar to those of other eucrites, although its Fe and Ti content are slightly higher and Mg- content is slightly lower. In addition, the K- content of Lakangaon (0.06 wt%) is close to that of Stannern. They suggested all these peculiarities of Lakangaon with a low Mg* value of 0.334 to a late stage of crystallization of the eucritic melt from the magma ocean. The best parameter connected with the fractionation of basaltic melt is the Mg* [Molar MgO/ (MgO + FeO)], which varies between 0.37 and 0.43 for the majority of non-cumulate eucrites. In the ’80s, Warren et al. (1985, 1987) reported bulk analysis of major and selected incompatible trace elements for Lakangaon along with Nuevo Laredo (NL) and one Antarctic eucrite by INAA technique. They suggested that Lakangaon, with a low Mg* value of 0.336, is far more Fe-rich (most ferroan) than any other eucrites except perhaps Nuevo Laredo, with a low Mg* value of 0.326. They, after a review of the literature data, considered most of the MG (Main Group) eucrites to belong to the NL trend besides the ST (Stannern) trend. According to them, the members of the NL trend (Nuevo Laredo, Lakangaon etc.), with 1.4 times the Ti and other incompatible elements, are not primary but formed out of residual liquid from fractional crystallization, whereas the

members of the ST trend (Stannern, Bouvante etc.) characterized by unusually high Ti and incompatible elements but with normal Mg* (0.4) might have formed by a low degree of melting. We find another complete bulk analysis of Lakangaon along with 15 other eucrites by ICP-AES and ICP-MS technique in Barrat et al. (2000). They concluded that no cumulate and non-cumulate eucrites represent primary melt; all eucrites are produced from 'in-situ crystallization' a differentiated magma ocean of a small asteroid body under low gravity environment.

Petrogenesis

During the last six decades, several petrogenetic models for eucrites have been put forward in the literature since Mason (1962) proposed the 'fractional crystallization model'. He described the origin of eucrites from residual liquids after extensive fractional crystallization of a more magnesian magma, which had earlier produced diogenites as cumulate partners. In contradiction, the 'partial melting model' by Stolper (1977) introduced the origin of most of the eucrites as the primary partial melts of a primitive metal-free chondritic precursor, and it was confirmed using the REE data by Consolmagno and Drake (1977). With the availability of an extensive set of bulk major, minor and trace element data, Hsu and Crozaz (1996) suggested that the bulk REE concentrations and other incompatible elements are strongly controlled by minor phases like phosphates, ilmenite and zircon. Different degrees of partial melting of a chondritic source account for the Stannern and Main Group trends, and its fractional crystallization is responsible for the Nuevo Laredo trend. The 'Layered Crust Model' of a magma ocean by Takeda (1997) proposed the successive generation of diogenite, cumulate eucrite, and basaltic eucrite, respectively, through crystal fractionation in sequence. Summing up the substantial data on eucrite petrochemistry over the decades, the evolved models are (a) partial melting of a chondritic precursor, (b) Total melting followed by fractional

crystallization of a magma ocean, (c) Total melting followed by equilibrium crystallization of a magma ocean, and (d) In-situ crystallization of a differentiated magma ocean.

The partial melting model is incapable of explaining the correlation between W (moderately siderophile) and La (lithophile) and very low siderophile elements besides the time and physical conditions required for the core formation and the early igneous activity of the HED parent body (Srinivasan et al., 1999). The equilibrium crystallization model makes accommodating extremely incompatible element fractionation difficult, as observed in diogenitic orthopyroxene. If the same magma ocean is considered the source of eucrite and diogenite, all non-cumulate eucrites including Stannern trend members must represent residual melts produced in the magma chamber (Warren, 1998). The fractional crystallization model may be ruled out as it cannot explain a common process for both the Stannern and Nuevo Laredo trends of eucrites. Barrat et al. (2000) advocated for Langmuir's 'in situ crystallization model' (1989), which explains that both cumulate and non-cumulate eucrites are genetically related. Trace element data of non-cumulate eucrites are inappropriate to justify both the equilibrium and fractional crystallization models. This *in situ* model accommodates most of the chemical features of non-cumulate eucrites, especially the decoupling between the major elements and incompatible trace elements. Moreover, this model explains the Stannern and Nuevo Laredo trends as the heterogeneities of *in situ* crystallization regimes within a magma ocean rather than their evolution by two different fractionation processes of partial melting and fractional crystallization, respectively.

Based on textural attributes and whole-rock composition, we assign Lakangaon as a basaltic eucrite with some dissimilarities. Texturally, it nowhere shows fine-grained, ophitic-subophitic intergrowths of pigeonite and plagioclase, typical of non-cumulate ordinary eucrites. Geochemically, it is extremely iron-rich basalt in bulk composition with the lowest Mg* values, analogous to Nuevo Laredo eucrite (Table 4). Being a monomict eucrite breccia, petrography

of the Lakangaon sample comprises of tectonically reworked lithic clasts (max size of 1.5 mm × 1.2 mm) of pyroxene-dominated gabbroic basalt similar to equilibrated cumulate eucrite and these clasts are sparsely distributed in crushed as well as pulverized matrix of basaltic mineralogy (Fig. 2). Lakangaon reflects the textural signatures of two-stage thermal recrystallizations, once during post-crystallization and the other during the post-brecciation event. Subangular to subrounded clasts of gabbroic hornfels texture, along with two subsets of exsolved pyroxenes (Fig. 6) and bytownite- anorthite plagioclase, marks the Type 6 thermal metamorphism of Takeda and Graham (1991). Further coarsening of gabbroic components, extensive clouding of gabbroic pyroxenes with troilite beads, and clouding of plagioclase with pyroxene-ilmenite-chromite inclusions in the form of healed cracks and crystal lattices mark the textural manifestations of post-brecciation thermal event. Overprints of two thermal events obliterated the primary igneous textural properties of Lakangaon and induced a cumulate texture of secondary origin. The Fe-rich fractionated basaltic melt of Lakangaon eucrite, as evident from Fe-rich pyroxene composition following the NL trend, was further enriched with Fe and Ti concentration during the formation of clouding texture in the post-brecciation subsolidus reheating event (Fig. 6).

Troilite and silica inclusions could have played a reducing agent role in typical basaltic eucrite pyroxene compositions. The inclusions of troilite and silica in pyroxenes were explained by Zhang et al. (2013) using this fundamental type of reaction, where the reactants were S vapor and eucritic pyroxene instead of fayalite. In Juvinas, Nuevo Laredo, Sioux County, and Stannern, Duke (1963) reported petrographic evidence for the late-magmatic stage reaction of pyroxene to form troilite and silica; nonetheless, he attributed this to late-stage S vapor. He further discussed that the late-stage ferroan pigeonite and augite are clouded by troilite inclusions, in contrast to the largely inclusion-free pyroxene cores in Pasamonte. In this example, Duke (1963) found no evidence for the interaction of pyroxene with S vapor to form

troilite, suggesting that the co-crystallization of these two phases from magma for this meteorite is plausible.

The petrography of the clast and matrix of Lakangaon eucrite shows an equilibrated high Fe-rich pyroxene phase, unequilibrated bytownite and anorthite plagioclase phase and relict signature of distinctively gabbroic texture are more consistent with a cumulate basaltic magma whereas the whole-rock composition of Lakangaon along with its well defined linear pyroxene compositional trend parallel to that of Nuevo Laredo assign a non-cumulate basaltic character. Therefore, a mixed signature of cumulate (from texture) and non-cumulate (from bulk major element composition) characters of Lakangaon needs a justification for its thermal and metamorphic evolution.

We propose a simple evolutionary model for the Lakangaon eucrite, which crystallized in situ at a late stage from a differentiated residual mafic magma analogous to the 'Layered Crust Model' of a magma ocean by Takeda (1997) and 'In-situ crystallization of a differentiated magma ocean model' of Barrat et al. (2000). The end product of the primary igneous processing in Lakangaon had been transformed due to subsequent effects of impact metamorphism and thermal metamorphism in successive stages similar to multiphase thermal and impact events described by Metzler (1995) (Fig. 11).

1. We find an igneous texture of crystallization from an iron-enriched mafic melt for Lakangaon.
2. Evidence of slow subsolidus cooling and heating in Lakangaon is indicated by the inversion of Fe-pigeonite to Fe-orthopyroxene and the exsolution of ferroaugite lamellae in pigeonites.
3. The in-situ, late-stage crystallization of Lakangaon from differentiated magma ocean was disturbed to some extent due to the effect of impact brecciation, and it is inferred from the

textural signature of kink bands in exsolved pyroxenes caused by flexure-slip deformation. This impact event was also responsible for the random mechanical mixing of impact clasts as well as the comminution of grains. The absence of melt clast breccias and shock-melt veins in Lakangaon confirms the fact that the impact-processed igneous crust was sampled from a megaregolith segment below the crater margin and not from the deep crater floor.

4. The first signature of thermal metamorphism was the recrystallization textures in the clasts in the form of triple points, equant grain habits, and compositional equilibration in pyroxenes. The effect of thermal metamorphism was not strong enough to equilibrate the plagioclase grains, as observed from subtle compositional differences between the clasts and those of the matrix.
5. A second episode of impact brecciation and subsequent thermal metamorphism is overprinted in Lakangaon for the complete absence of any fine-grained basaltic clasts showing ophitic-subophitic intergrowths, coarsening of grain size in larger clasts, the appearance of granulitic and hornfelsic intergrowths and clouding in pyroxenes as well as plagioclase with the dust of minor minerals like troilite, pyroxenes, silica, chromites, and ilmenites.

Conclusion

We conclude that Lakangaon eucrite is extensively recrystallized monomict fragmental breccias of an asteroid parent body (probably similar to other HEDs). The texture of the Lakangaon breccia reflects a polyphase, post-igneous history of thermal and impact metamorphism in the coarse-grained lithic and mineral clasts of variable size embedded in a finer recrystallized clastic matrix of similar mineralogy. All the lithic clasts are coarse-grained, gabbroid textured with some granulitic hornfels mosaic look, heavily fractured with subsequent healing recoveries; signatures of brittle rupturing and displacements and prominent kink bands due to flexure slip deformation in the exsolution lamellae of pyroxenes are noted in the mineral

clasts. Neither any clast of impact melt nor any textural evidence of melt quenching was observed. The lack of Ni-free iron beads or Ni-bearing metal grains along with a low abundance of siderophile elements in Lakangaon rules out the possibility of any chondritic contamination. Lakangaon shows two types of alterations: mechanical mixing during impact and thermal alterations before, during, and after the impact event. Signatures of at least two phases of impact history are recorded: (a) first one during the waning phase of igneous crystallization when equilibrated pyroxenes with structural inversions from pigeonite to orthopyroxene due to a brief period of reheating, pigeonite with exsolved augite lamellae due to slow subsolidus cooling and ductile to brittle fracturing in the pyroxenes and plagioclase clasts occurred (b) second impact phase during the post-crystallization period when comminution of fractured clasts took place along with the vapourization of troilites. Post-impact thermal annealing made the coarsening of recrystallized clasts, the formation of granulitic hornfels textures in the clasts, the healing of earlier cracks and fractures within the clasts, and finally the formation of clouding textures in both pyroxene and plagioclase with mainly finer inclusions of the minor minerals; Sulphur vapor played a significant role as a transport medium for the extensive development of clouding texture at a late stage.

Acknowledgment

We acknowledge Department of Space (Govt. of India) for financial help.

List of Figures

Fig.7. Feldspar triangular diagram showing the two compositional plots of clast feldspars and matrix feldspars.

Fig.8. Mode of occurrences of minor minerals in Lakangaon (a) conjugate ilmenite- chromite grains (b) zircon grains in association with ilmenite

Fig.9. TiO_2 vs FeO* / Mgo plots from Lakangaon eucrite showing clusters of Stannern trend and Neuvo Laredo trend. Literature data from Mittlefehldt (2015) and references therein.

Fig.10. Chondrite normalized REE - pattern of Lakangaon eucrite. Data from Moore County and Nuevo Laredo are incorporated for comparison.

Fig. 11. Evolutionary model of thermal and impact metamorphic evolution of Lakangaon eucrite (modified after Metzler et al., 1992). (a) source Fe-rich mafic melt as primary magma, (b) crystallization of primary magma, (c) slow subsolidus cooling, inversion of Fe pigeonite, ferroaugite lamellae in pigeonite, (d) first signature of impact brecciation, kink band in lamellae. (e) first thermal metamorphism; recrystallisation and (f) second signature of impact followed by thermal metamorphism; granulite, hornfelsic intergrowth, clouding of pyroxene,

Table Captions

Table 1. Representative EPMA analyses of Lakangaon pyroxenes

Table 2. Representative EPMA analyses of Lakangaon plagioclase

Table 3. Representative analyses of accessory minerals (ilmenite and chromite)

Table 4. Whole rock elemental composition of Lakangaon eucrite (Literature data from Nuevo Laredo and Moore County Barrat et al. 2007). Normalised data from McDonough and Sun, 1995.

References

Barrat, J. A., Blichert-Toft, J., Gillet, P., & Keller, F. (2000). The differentiation of eucrites: the role of in situ crystallisation. Meteoritics & Planetary Science, 35(5), 1087-1100.

Barrat, J. A., Jambon, A., Bohn, M., Blichert-Toft, J., Sautter, V., G¨opel, C., ... & Keller, F. (2003). Petrology and geochemistry of the unbrecciated achondrite Northwest Africa 1240 (NWA 1240): An HED parent body impact melt. Geochimica et Cosmochimica Acta, 67(20), 3959-3970.

Barrat, J. A., Yamaguchi, A., Greenwood, R. C., Bohn, M., Cotten, J., Benoit, M., & Franchi, I. A. (2007). The Stannern trend eucrites: Contamination of main group eucritic magmas by crustal partial melts. Geochimica et Cosmochimica Acta, 71(16), 4108-4124.

Consolmagno, G. J., & Drake, M. J. (1977). Composition and evolution of the eucrite parent body: Evidence from rare earth elements. *Geochimica et Cosmochimica Acta*, *41*(9), 1271-1282.

Coulson, A. L. (1940). A Catalogue of Meteorites, Memoirs of the Geological Survey of India, 75, 1940.

Duke, M. B. (1963). *Petrology of the basaltic achondrite meteorites* (Doctoral dissertation, California Institute of Technology).

Duke, M. B., & Silver, L. T. (1967). Petrology of eucrites, howardites and Mesosiderites. Geochimica et Cosmochimica Acta, 31(10), 1637-1665.

Dymek, R. F., Albee, A. L., Chodos, A. A., & Wasserburg, G. J. (1976). Petrography of isotopically-dated clasts in the Kapoeta howardite and petrologic constraints on the evolution of its parent body. Geochimica et Cosmochimica Acta, 40(9), 1115-1130.

Gooding, J. L. (1986). Clay-mineraloid weathering products in Antarctic meteorites. *Geochimica et Cosmochimica Acta*, *50*(10), 2215-2223.

Haba, M. K., Yamaguchi, A., Horie, K., & Hidaka, H. (2014). Major and trace elements of zircons from basaltic eucrites: Implications for the formation of zircons on the eucrite parent body. Earth and Planetary Science Letters, 387, 10-21.

Harlow, G. E. & Klimentidis, R. (1980). Clouding of pyroxene and plagioclase in eucrites: Implications for post-crystallization processing. Lunar and Planetary Science 11, Lunar and Planetary Institute, Houston Texas, USA, 1131-1143.

Hsu, W., & Crozaz, G. (1996). Mineral chemistry and the petrogenesis of eucrites: I. Noncumulate eucrites. Geochimica et Cosmochimica Acta, 60(22), 4571-4591.

Krinov, E. L. (1960). The Tunguska Meteorite. *International Geology Review*, *2*(1), 8-19.

Langmuir, C. H. (1989). Geochemical consequences of in situ crystallization. *Nature*, *340*(6230), 199-205.

Mason, B. (1962). Meteorites. Wiley, New York, 274 pp.

McCarthy, T. S., Erlank, A. J., Willis, J. P., & Ahrens, L. H. (1974). New chemical analyses of six achondrites and one chondrite. Meteoritics, 9(3), 215-221.

McDonough, W. F., & Sun, S. S. (1995). The composition of the Earth. Chemical geology, 120(3-4), 223-253.

McSween Jr, H. Y., Binzel, R. P., De Sanctis, M. C., Ammannito, E., Prettyman, T. H., Beck, A. W., ... & Dawn Science Team. (2013). Dawn; the Vesta–HED connection; and the geologic context for eucrites, diogenites, and howardites. Meteoritics & Planetary Science, 48(11), 2090-2104.

Meteoritic Bulletin (2006, v.7.1)

Metzler K., Bobe K., Palme H., Spettel B., and Sto¨ffler D. (1995) Thermal and impact Metamorphism on the HED parent asteroid. Planet. Space Sci. 43, 499–525.

Mittlefehldt, D. W. (2015). Asteroid (4) Vesta: I. The howardite-eucrite-diogenite (HED) clan of meteorites. *Geochemistry*, *75*(2), 155-183.

Mittlefehldt, D. W., Greenwood, R. C., Berger, E. L., Le, L., Peng, Z. X., & Ross, D. K. (2022). Eucrite- type achondrites: Petrology and oxygen isotope compositions. *Meteoritics & Planetary Science*, *57*(2), 484-526.

Miyamoto, M., Takeda, H., & Yanai, K. (1978). Yamato achondrite polymict breccias.

Srinivasan, G., Goswami, J. N., & Bhandari, N. (1999). 26Al in eucrite Piplia Kalan: Plausible heat source and formation chronology. Science, 284(5418), 1348-1350.

Stolper, E. (1977). Experimental petrology of eucritic meteorites. Geochimica et Cosmochimica Acta, 41(5), 587-611.

Takeda, H. (1997). Mineralogical records of early planetary processes on the howardite, eucrite, diogenite parent body with reference to Vesta. Meteoritics & Planetary Science.

Takeda, H., & Graham, A. L. (1991). Degree of equilibration of eucritic pyroxenes and thermal metamorphism of the earliest planetary crust. *Meteoritics*, *26*(2), 129-134.

Warren, P. H. (1998). Howardite-eucrite-diogenite magma ocean petrogenesis: Equilibrium or fractional crystallization?. *Meteoritics & Planetary Science, vol. 33, p. A162*, *33*, A162.

Warren, P. H., & Jerde, E. A. (1987). Composition and origin of Nuevo Laredo trend eucrites. Geochimica et Cosmochimica Acta, 51(3), 713-725.

Warren, P. H., Kallemeyn, G. W., & Jerde, E. A. (1985). Geochemistry of Lakangaon, the Most Fe-Rich Eucrite. Meteoritics, 20, 779.

Zhang, A. C., Wang, R. C., Hsu, W. B., & Bartoschewitz, R. (2013). Record of S-rich vapors on asteroid 4 Vesta: Sulfurization in the Northwest Africa 2339 eucrite. Geochimica et Cosmochimica Acta, 109, 1-13.

Figure 1

Fig. 1: Hand specimen view of the Lakangaon main mass showing the overall shape of the trigonal pyramid; faces are covered with highly glossy, netted, pitch dark fusion crust and faint markings of flowage lines.

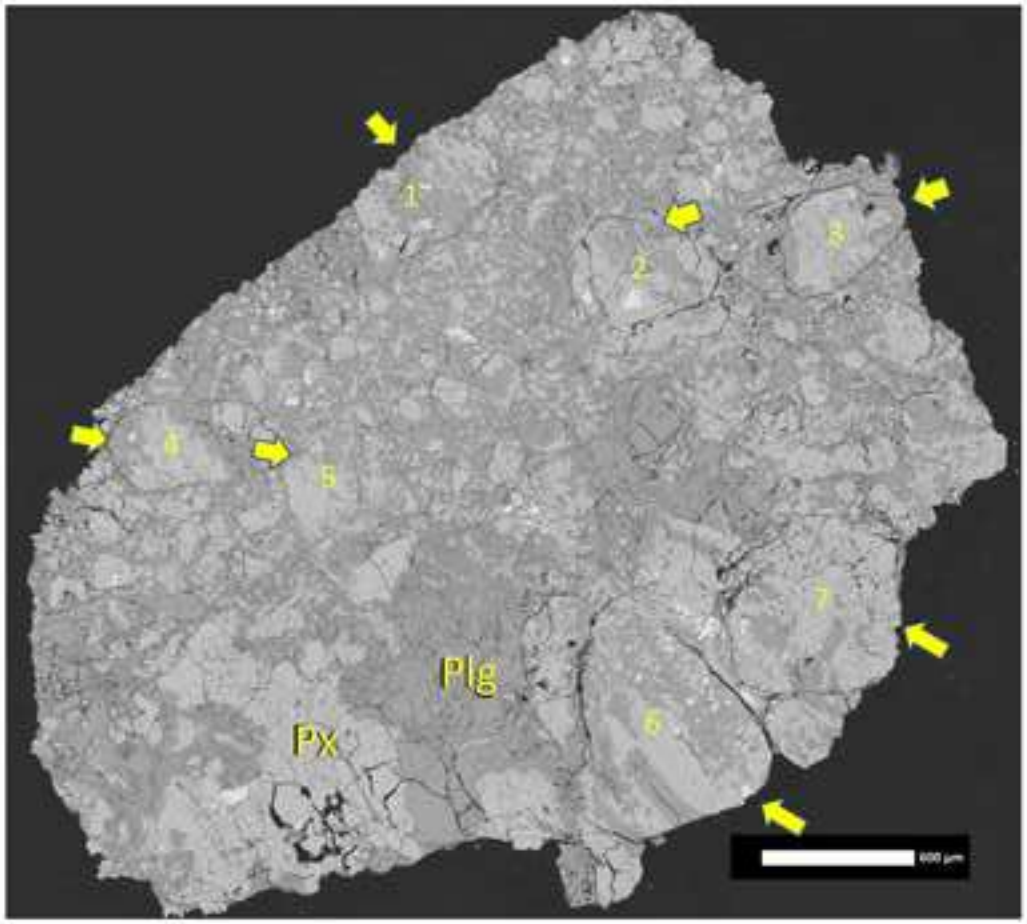

Fig.2. Mosaic view of BSE images of two polished sections (a and b) of Lakangaon eucrite. Note the subangular to subrounded nature of larger lithic clasts (marked A to F in section 'a') embedded in a clastic silicate matrix which is partly crystalline to recrystallized. Note the fracturing and cataclastic appearances around the clast peripheries and the development of pulverized zones in the matrix at the intersection of fracture planes.

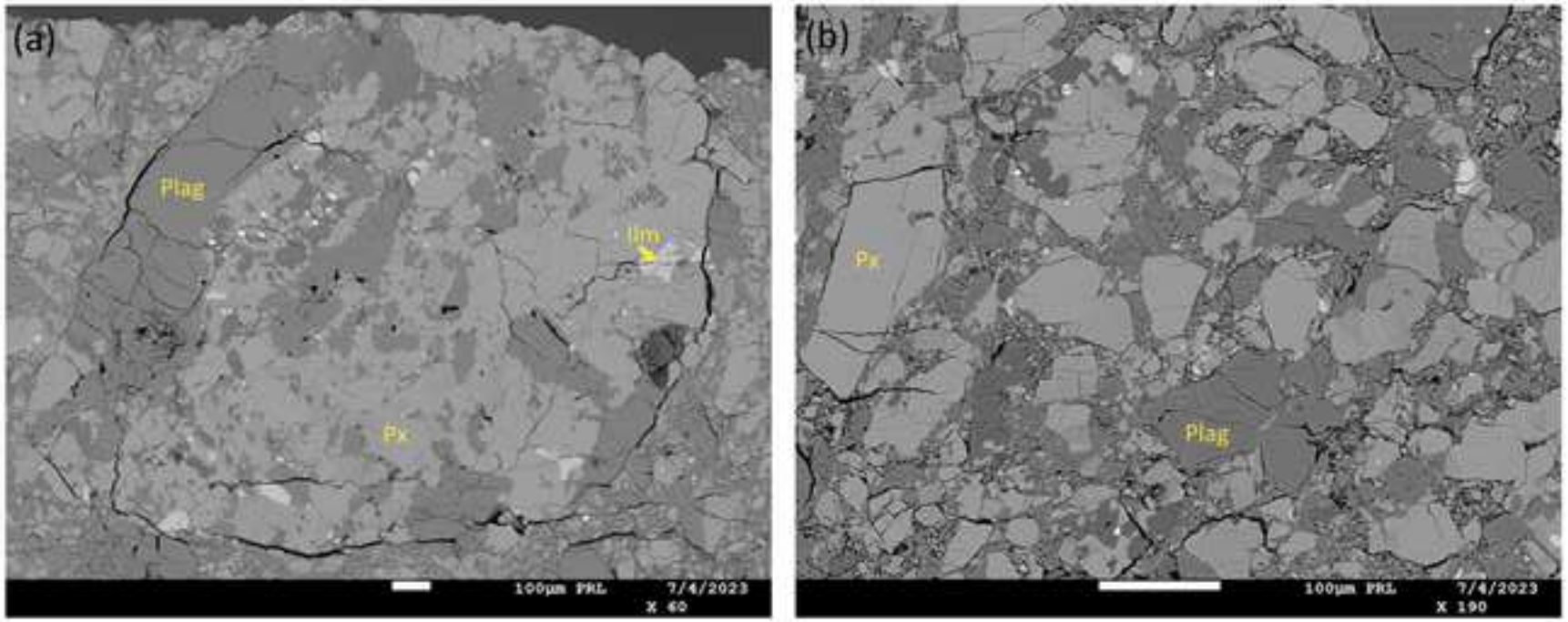

Fig. 3. BSE image of (a) Clast and (b) matrix. Plag: Plagioclase, Px:Pyroxene, Ilm: Ilmenite

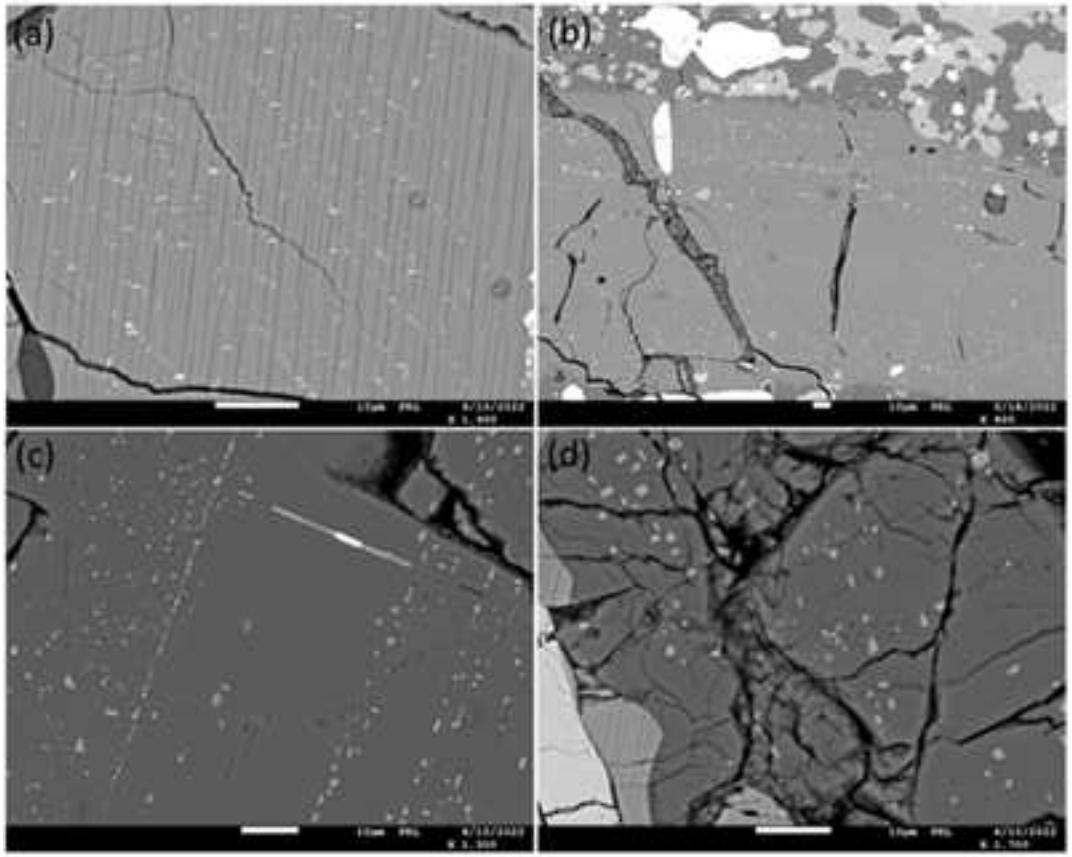

Fig. 4. (a) BSE images that show clouding in pyroxenes from Lakangaon; the clouding-causing minerals are thin and rod-shaped and are mostly aligned in one direction. The inclusions range from 0.2 × 0.05 μm to 1.8 × 0.5 μm.

(b) BSE images that show clouding in plagioclases from Lakangaon; this clouding is very dense and different from those of pyroxene, where the variation in the size of clouding-causing inclusions is not huge. The inclusions are bigger in size towards the edge of the plagioclase (average ~ 0.6 × 0.4 μm) and are extremely small around the centre of the plagioclase grain (~ 0.4 × 0.2 μm). A streak (appears like a finely dotted line) made of very fine inclusions can also be seen going through the centre of the plagioclase grain.

(c) BSE images of clouding in plagioclase that show inclusions of various sizes (average ~ 1.1 × 1.3 μm), from almost circular to triangular and even rectangular. Again, a vertical streak of inclusions can be seen. The bright white euhedral phase is troilite (~ 5.3 × 0.1 μm), which has pyroxenes on both sides (~ 11.3 × 0.1 μm on the left side). Notice how even this tiny bit of pyroxene shows both augite and pigeonite.

(d) BSE image of clouding in plagioclase shows a horizontal streak made by fine silica inclusions. Another interesting observation would be that the centre of plagioclase is void of any fractures and is also void of any clouding.

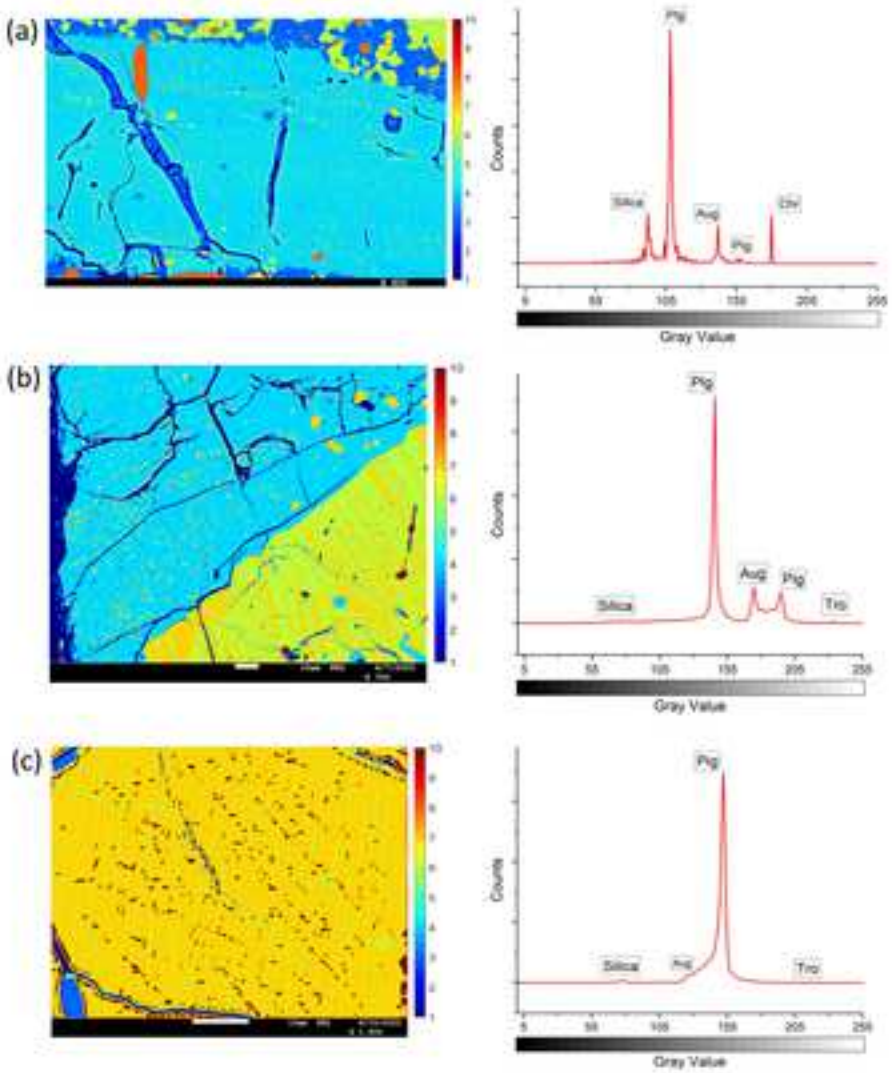

Fig. 5. Segmented Images of Lakangaon.

(a) The major clouding-causing agent in plagioclase is augite (light green), including the straight line/streak. Some inclusions form two to three curve lines, and these inclusions are silica (sapphire blue). A few inclusions are of pigeonite (yellow). The small inclusions that are in close proximity to the big troilite inclusion (~ 7 x 5 µm) are also troilite (brown).

(b) This image shows clouding in plagioclase as well as in pyroxene. The plagioclase is majorly clouded by plagioclase and silica in about equal proportion, but very few inclusions of troilite are also present together in clusters, especially in the part of plagioclase which is closer to the pyroxene grain. Some pyroxene inclusions in plagioclase exhibit both augite and pigeonite. The exsolved pyroxenes, on the other hand, are solely clouded by troilite in this case.

(c) Extensive clouding by troilite in the exsolved pyroxenes (very fine exsolved lamellae of augite in pigeonite) of Lakangaon.

Figure 6

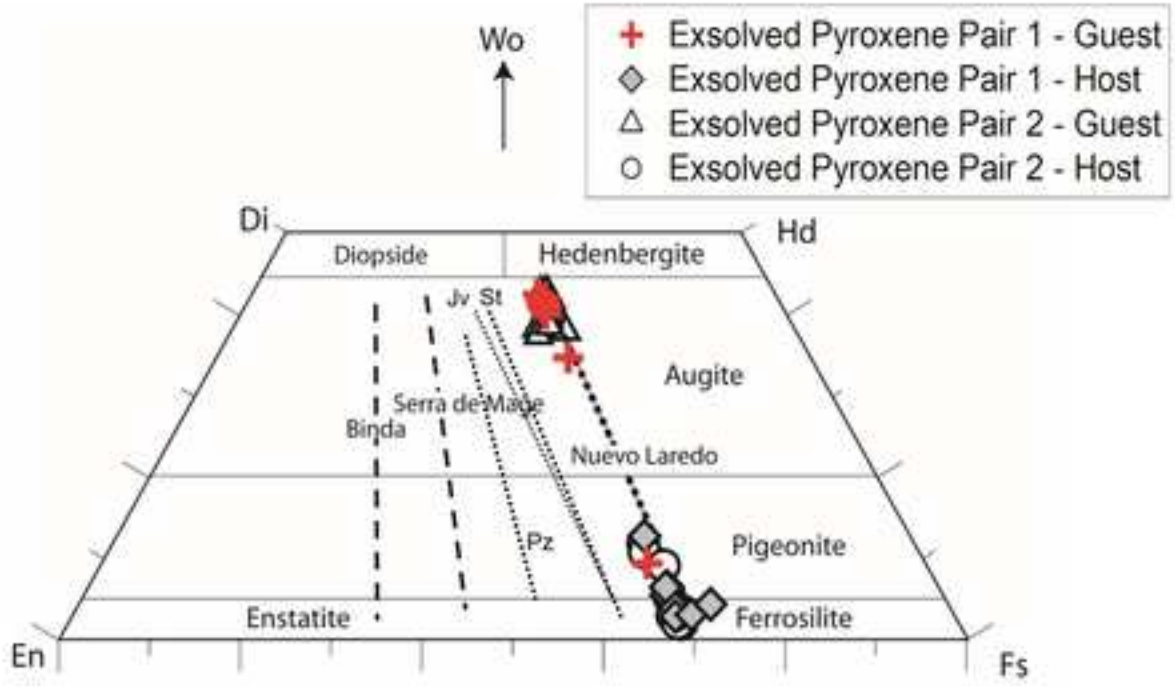

Fig. 6. Pyroxene quadrilateral diagram showing two distinct clusters of co-existing low-Ca pyroxenes (Fe-orthopyroxene and Fe-pigeonite) and high-Ca pyroxenes (Fe-augite). Jv: Juvinas, St: Stannern, Pz: Pomozdino. Pyroxene data from Barrat et al. 2007.

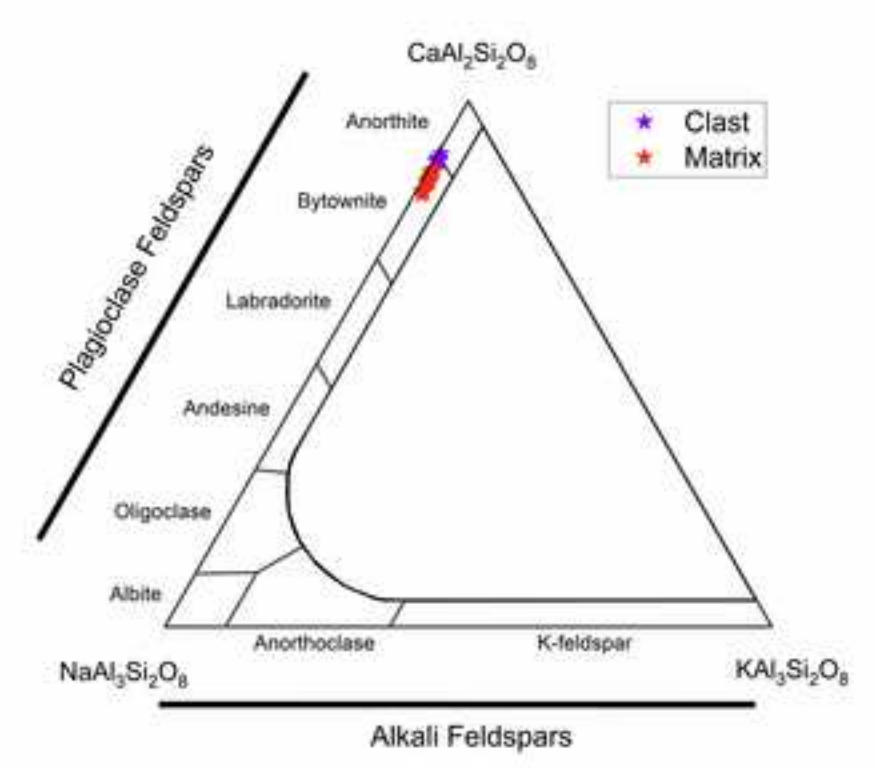

Fig. 7. Feldspar triangular diagram showing the two compositional plots of clast feldspars and matrix feldspars.

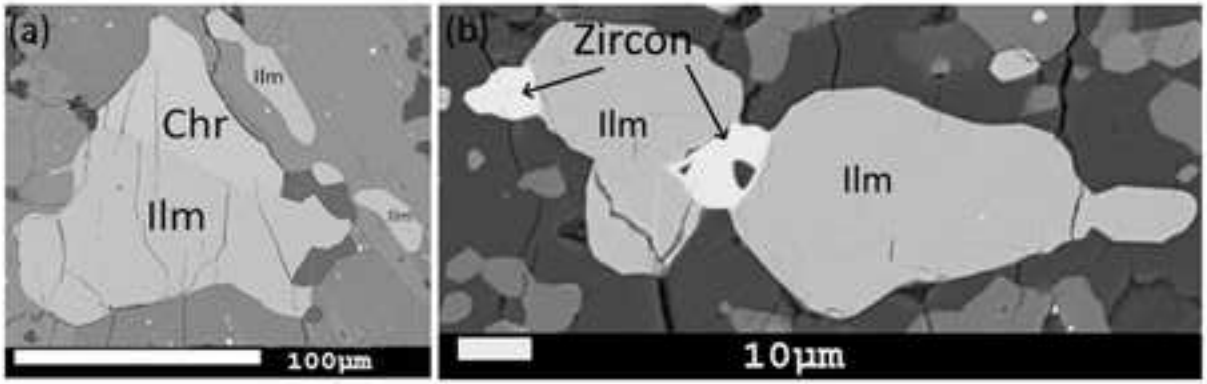

Fig.8. Mode of occurrences of minor minerals in Lakangaon (a) conjugate ilmenite- chromite grains (b) zircon grains in association with ilmenite.

Please write red circle with black outline: Lakangaon, this study

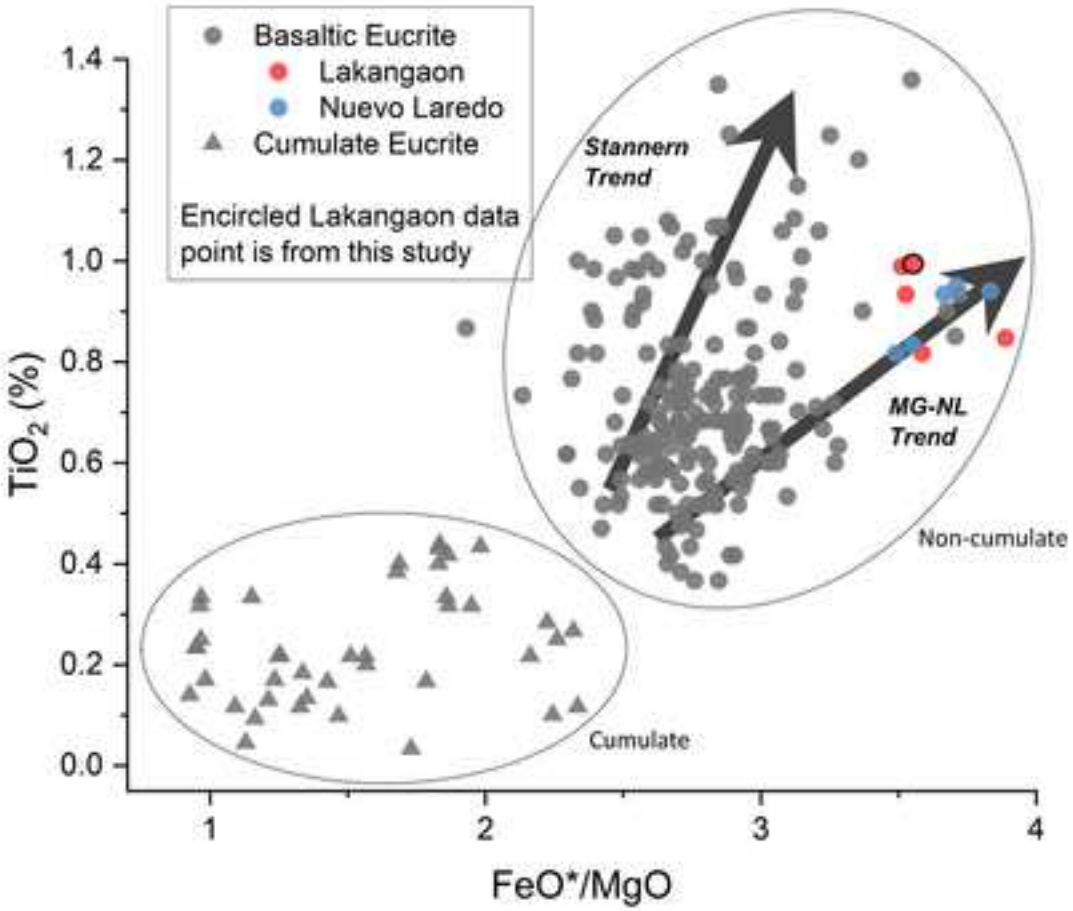

Fig.9 TiO_2 vs FeO* / MgO plots from Lakangaon eucrite showing clusters of Stannern trend and Neuvo Laredo trend. Cumulate and non-cumualte data from Mittlefehldt (2015) and references therein.

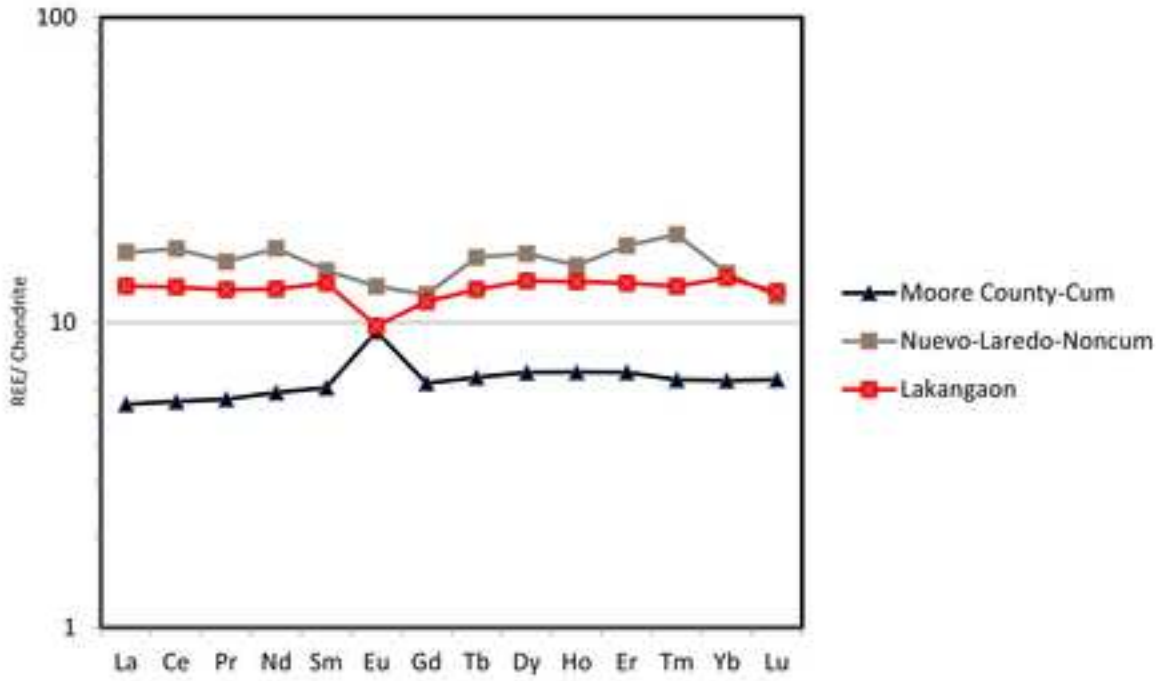

Fig. 10 Normalised REE plot of Lakangaon and Moore County (cumulate) and Nuevo Laredo (non cumulate) eucrites.

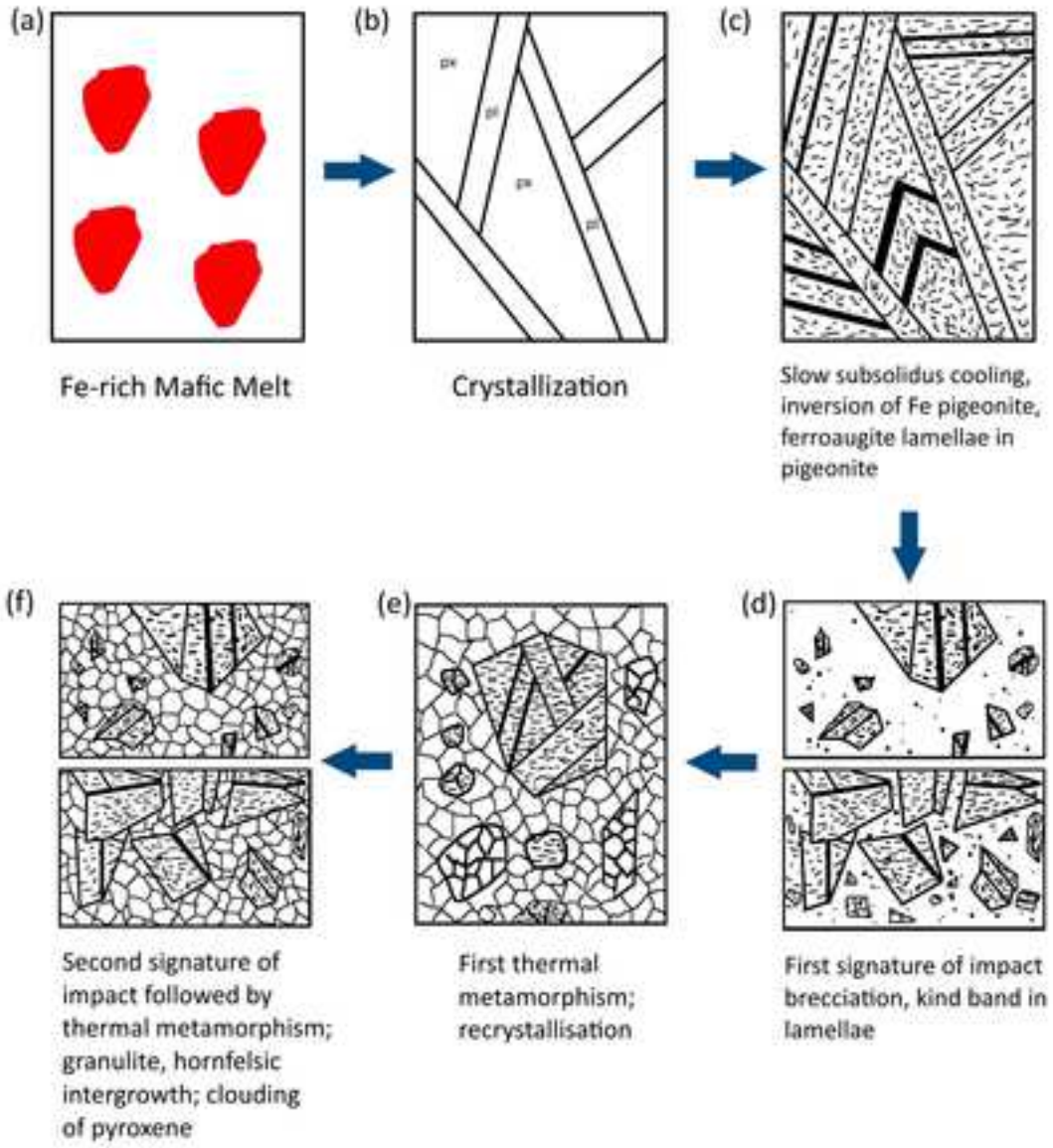

Fig. 11. Evolutionary model of thermal and impact metamorphic evolution of Lakangaon eucrite (modified after Metzler et al., 1992). (a) Source Fe-rich mafic melt as primary magma, (b) crystallization of primary magma, (c) slow subsolidus cooling, inversion of Fe pigeonite, ferroaugite lamellae in pigeonite, (d) first signature of impact brecciation, kink band in lamellae (e) first thermal metamorphism; recrystallisation and (f) Second signature of impact followed by thermal metamorphism; granulite, hornfelsic intergrowth, clouding of pyroxene,

Table 1. Representative EPMA analyses of Lakangaon Pyroxene

	Pyroxene I				Pyroxene II			
	N=18			Avg(SD)	N=16			Avg (SD)
SiO_2	49.78	48.78	48.68		51.22	50.60	50.80	
TiO_2	0.15	0.17	0.15		0.24	0.25	0.30	
Al_2O_3	0.26	0.19	0.20		0.41	0.43	0.46	
Cr_2O_3	0.06	0.09	0.07		0.24	0.21	0.20	
FeO	35.24	37.10	38.29		21.01	22.55	20.30	
MnO	1.06	0.56	0.25		0.68	1.43	1.22	
MgO	9.53	9.06	9.40		8.70	8.41	8.51	
CaO	4.83	3.31	1.79		18.75	16.94	18.70	
Na_2O	n.d.	n.d.	n.d.		n.d.	n.d.	n.d.	
K_2O	n.d.	n.d.	n.d.		n.d.	n.d.	n.d.	
Total	100.91	99.21	98.84		101.25	100.82	100.49	
Cations based on 6 oxygens								
Si	1.990	1.994	1.998		1.982	1.980	1.981	
Ti	0.004	0.005	0.005		0.007	0.007	0.009	
Al	0.012	0.009	0.010		0.019	0.020	0.021	
Cr	0.002	0.001	0.002		0.007	0.007	0.006	
Fe	1.178	1.268	1.314		0.680	0.738	0.662	
Mn	0.036	0.019	0.009		0.022	0.047	0.040	
Mg	0.568	0.552	0.575		0.502	0.490	0.495	
Ca	0.207	0.145	0.079		0.778	0.710	0.782	
Catsum	3.998	3.995	3.991		3.997	4.000	3.996	
Wo (mol%)	1.95	7.38	4.00	4.21(2.39)	39.68	36.64	40.32	37.81(3.06)
En	32.88	28.08	29.22	29.43(0.57)	25.60	25.30	25.51	25.81(0.60)
Fs	60.32	64.54	66.78	66.36(2.10)	34.71	38.07	34.16	36.38(2.66)

N=number of analyses, n.d. not determined, Avg: Average, SD: Standard Deviation, Pyroxene types based on FeO content

	Pyroxene III				Pyroxene IV			
	N=8			Average (SD)	N=8			Avg (SD)
SiO2	50.73	50.57	50.66		49.90	49.87	49.66	
TiO2	0.23	0.21	0.27		0.16	0.16	0.15	
Al2O3	0.60	0.32	0.39		0.27	0.20	0.16	
Cr2O3	0.13	0.09	0.16		0.11	0.14	0.12	
FeO	28.52	29.96	26.72		35.37	34.09	31.75	
MnO	1.07	0.50	0.47		1.31	1.31	0.70	
MgO	9.15	9.30	9.11		9.54	9.42	9.40	
CaO	11.42	10.36	13.40		4.21	5.11	7.27	
Na2O	n.d.	n.d.	n.d.		n.d.	n.d.	n.d.	
K2O	n.d.	n.d.	n.d.		n.d.	n.d.	n.d.	
Total	101.81	101.31	101.19		100.86	100.29	99.21	
Cations based on 6 oxygens								
Si	1.981	1.989	1.983		1.995	2.000	2.001	
Ti	0.007	0.006	0.008		0.005	0.005	0.005	
Al	0.028	0.015	0.018		0.012	0.009	0.008	
Cr	0.004	0.003	0.005		0.003	0.004	0.004	
Fe	0.932	0.985	0.875		1.183	1.143	1.070	
Mn	0.035	0.017	0.016		0.044	0.045	0.024	
Mg	0.533	0.545	0.532		0.568	0.563	0.565	
Ca	0.478	0.437	0.562		0.180	0.220	0.314	
Catsum	3.997	3.996	3.998		3.992	3.989	3.989	
Wo (mol%)	24.60	22.20	28.56	28.48(5.38)	9.34	11.41	16.10	14.76(3.48)
En	27.43	27.70	27.01	26.95(0.59)	29.42	29.23	28.98	29.09(0.45)
Fs	47.97	50.10	44.44	44.57(4.91)	61.24	59.36	54.92	56.15(3.19)

n.d. not determined, Avg: Average, SD: Standard Deviation, Pyroxene types based on FeO content

Table 2 Representative EPMA analyses of Lakangaon Plagioclase

	Plagioclase (within clast)				Plagioclase (within matrix)			
	N=11			Avg (SD)	N=5			Avg (SD)
SiO_2	47.10	47.06	47.35		46.96	47.39	47.44	
TiO_2	n.d.	n.d.	n.d.		0.06	0.03	n.d.	
Al_2O_3	33.38	33.84	33.44		33.90	33.76	33.72	
Cr_2O_3	0.08	0.04	n.d.		n.d.	n.d.	n.d.	
FeO	0.27	0.24	0.34		0.44	0.48	0.44	
MnO	n.d.	n.d.	n.d.		0.03	n.d.	n.d.	
MgO	0.01	0.03	n.d.		0.03	0.01	0.01	
CaO	19.05	18.91	18.86		18.07	17.96	17.78	
Na_2O	1.12	1.19	1.22		1.27	1.34	1.45	
K_2O	0.08	0.11	0.11		0.12	0.14	0.15	
Total	101.10	101.43	101.33		100.87	101.10	101.00	
Cations based on 8 oxygens								
Si	2.152	2.142	2.157		2.146	2.160	2.163	
Al	1.798	1.816	1.796		1.826	1.814	1.812	
Cr	0.003	0.001	n.d.		n.d.	n.d.	n.d.	
Fe	0.010	0.009	0.013		0.017	0.018	0.017	
Mn	n.d.	n.d.	n.d.		0.001	0.000	n.d.	
Mg	0.001	0.002	n.d.		0.002	0.000	0.001	
Ca	0.933	0.922	0.921		0.885	0.877	0.869	
Na	0.099	0.105	0.108		0.113	0.118	0.128	
K	0.005	0.006	0.007		0.007	0.008	0.009	
Catsum	5.000	5.005	5.002		4.999	4.996	4.999	
An(mol%)	89.99	89.22	88.95	88.26(1.27)	88.12	87.38	86.38	86.63(1.39)
Ab	9.54	10.18	10.41	11.11(1.18)	11.21	11.79	12.76	12.54(1.36)
Or	0.47	0.60	0.64	0.63(0.13)	0.67	0.84	0.86	0.83(0.11)

N=number of analyses, n.d. not determined, Avg: Average, SD: Standard Deviation

Table 3. Representative EPMA analyses of accessory phases (Ilmenite and Chromite)

	Ilmenite		Chromite	
	N=8		N=19	
SiO_2	0.09-0.57		0.06-0.55	
TiO_2	52.74-53.66		10.19-14.66	
Al_2O_3	0.02-0.19		3.92-5.48	
Cr_2O_3	0.05-0.43		33.42-40.44	
FeO	45-46.14		42.22-45.59	
MnO	up to 1.29		0.17-1.32	
MgO	0.37-0.48		0.28-0.44	
CaO	0.41-0.64		0.14-0.47	
Na_2O	n.d.		n.d.	
K_2O	n.d.		n.d.	
Cr#(Cr+Al)	n.d.		0.62-0.66	

N=number of analyses, n.d. not determined

Table 4: Whole-rock data of Lakangaon (this study), non-cumulate eucrite (Nuevo Laredo) and cumulate eucrite (Moore County) from Barrat et al., 2007

	Lakangaon (this study)	Nuevo Laredo	Moore County
Fall/Find	Fall	Find	Fall
Lithology	Basaltic Eucrite	Basaltic Eucrite	Cumulate Eucrite
Trend	MGNL	MGNL	-
Petrologic type	Monomict	Monomict	-
Na (mg/g)	3.42	3.6	3.34
Mg	35.73	34.4	51.5
Al	55.68	65.42	78.18
Ca	65.83	77.9	70.04
Sc (µg/g)	34.31	35.8	19.8
Ti (mg/g)	5.96	5.6	2.58
V (µg/g)	54.02	60.1	n.a.
Cr	1.65	2.1	2.81
Mn (mg/g)	4.67	4.9	3.49
Fe (mg/g)	163.6	162.5	121.6
Co (µg/g)	5.06	2.87	11.3
Ni	5.5	3.7	4.2
Zn	17.29	1.17	3.4
Ga	1.63	1.69	1.6
Rb	511	370	60
Sr	66.75	84.4	70
Y	19.78	26.22	10.29
Zr	40.55	70	15.38
Nb	4.29	5.38	0.57
Ba	33.82	3.85	20.6
La	3.12	10.1	1.28
Ce	8.01	1.52	3.38
Pr	1.19	1.52	0.52
Nd	5.89	7.64	2.7
Sm	1.99	2.57	0.91
Eu	0.55	0.77	0.53
Gd	2.33	3.44	1.26
Tb	0.46	0.61	0.24
Dy	3.37	4.13	1.69
Ho	0.74	0.92	0.38
Er	2.16	2.67	1.1
Tm	0.33	n.a.	n.a
Yb	2.26	2.56	1.04
Lu	0.31	0.37	0.16
Hf	1.18	1.83	0.53
Pb (ng/g)	781	260	n.a.
Th	386	488	125
U	77	116	64
Eu/Eu*	0.78	0.79	1.5
#Mg	33.4	32.71	49.3

n.a. not available, MGNL: Main Group Nuevo Laredo

Declaration of Competing Interest

We confirm that this manuscript has not been published elsewhere and is not under consideration by another journal. All authors have approved the manuscript and agree with submission to Geochemistry. We have read and have abided by the statement of ethical standards for manuscripts submitted to Geochemistry. The authors have no conflicts of interest to declare.